Thin Solid Films 755 (2022) 139322

Contents lists available at ScienceDirect

Thin Solid Films

journal homepage: www.elsevier.com/locate/tsf

Linear and nonlinear optical properties of semi-elliptical InAs quantum dots: Effects of wetting layer thickness and electric field

B.O. Alaydin [a,c,*], D. Altun [a,b], E. Ozturk [c]

[a] Nanophotonic Application and Research Center, Sivas Cumhuriyet University, Sivas 58140, Turkey
[b] Department of Electricity and Energy, Sivas Vocational College, Sivas Cumhuriyet University, Sivas 58140, Turkey
[c] Department of Physics, Science Faculty, Sivas Cumhuriyet University, Sivas 58140, Turkey

ARTICLE INFO

Keywords:
Quantum dot
Indium arsenide
Gallium arsenide
Finite element method
Optical properties

ABSTRACT

In this paper, we have studied the optical properties of semi-elliptical InAs quantum dots (QDs) embedded in GaAs. Under effective mass approximation, the finite element method has been used to obtain wavefunctions and corresponding energy eigenvalues in three-dimension. It has been shown that the wetting layer (WL) thickness has a small effect on the (1-2) transition, but is more effective on the dipole moment matrix element (DMME) of the (2-3) and (1-3) transitions. It is seen that the linear absorption coefficients of the (2-3) and (1-3) transition reach the maximum at 4 A WL thickness. After that, we set the WL thickness to 4 A and we studied the effect of the electric field applied through the axial direction. The same as the WL effect, the electric field has caused a minor change in DMME of the (1-2) transition but it makes DMME of the (2-3) and (1-3) transitions stronger which results in very high linear absorption coefficients. For 20 kV/cm electric field intensity, the linear absorption coefficient reaches the maximum for the (2-3) and (1-3) transition.

1. Introduction

Improvements in semiconductor epitaxial growth technologies have enabled the manufacturing of more efficient, compact, and high-power photonic and optoelectronic devices such as lasers [1], light-emitting diodes [2], photodetectors [3], saturable absorbers [4]. Quantum well (QW), quantum well wire (QWW), and quantum dot (QD) heterojunctions are used as active mediums, where carrier transitions happen, in the structure of these sophisticated photonic devices. While QWs and QWWs have one-dimensional and two-dimensional confinements, QDs have three-dimensional confinement, which restricts the motion of carriers in all three-dimension [5–7]. Confinement is obtained by surrounding low bandgap material with high bandgap material and higher confinement improves the localization of carriers in low bandgap material [8]. This increases quantum production capability as well as lowers the interaction between carriers and interface quantum trap states. In addition to higher confinement, which leads to tunable linear and nonlinear optical properties, there is a strong dependence on QD shape and external fields as well, which modifies the optical properties.

In the literature, linear and nonlinear optical properties of QWs and wires have been studied extensively for many material and heterostructure shapes since the last two decades of the 20th century [9–14]. However, QDs are relatively new and under consideration mostly in the last two decades due to the superior absorption performances. Optical rectification and second harmonic generation in InAs/GaAs QD were investigated by Khaledi-Nasab et al. [15]. Third-order nonlinear optical susceptibility of QD with dielectric confinement was analyzed under an electric field by Cristea et al [16]. The nonlinear optical rectification in QD was examined by Xie [17]. El Haouari et. al looked into linear and nonlinear optical properties of single dopant in strained AlAs/GaAs QD [18]. Choubani et al. studied the nonlinear optical properties of lens-shaped InAs/GaAs QD considering the wetting layer (WL) [19]. Sargsian et al. researched linear and nonlinear optical properties of cylindrical InAs QD with modified Pöschl-Teller and Morse potentials under applied electric and magnetic fields [8]. Negatively charged trion in cylindrical QD was studied by Chnafi et al. [20]. Effect of laser field on double GaAs QD was shown by Maniero et. al [21]. Magnetic properties of an impurity in a parabolic GaAs QD were deeply discussed by Boda [22]. The optical properties of pyramidal QDs were simulated and comprehensively analyzed under electric and magnetic fields [23]. In most of these works, the WL effect was partially or not at all considered for sake of the simplicity to solve the Schrödinger equation in three-dimension. In addition, wavefunctions were obtained in one-dimension and only for the center of the QD. Apart from the center

* Corresponding author at: Nanophotonic Application and Research Center, Sivas Cumhuriyet University, Sivas 58140, Turkey.
E-mail address: balaydin@cumhuriyet.edu.tr (B.O. Alaydin).

https://doi.org/10.1016/j.tsf.2022.139322
Received 30 October 2021; Received in revised form 30 May 2022; Accepted 30 May 2022
Available online 6 June 2022

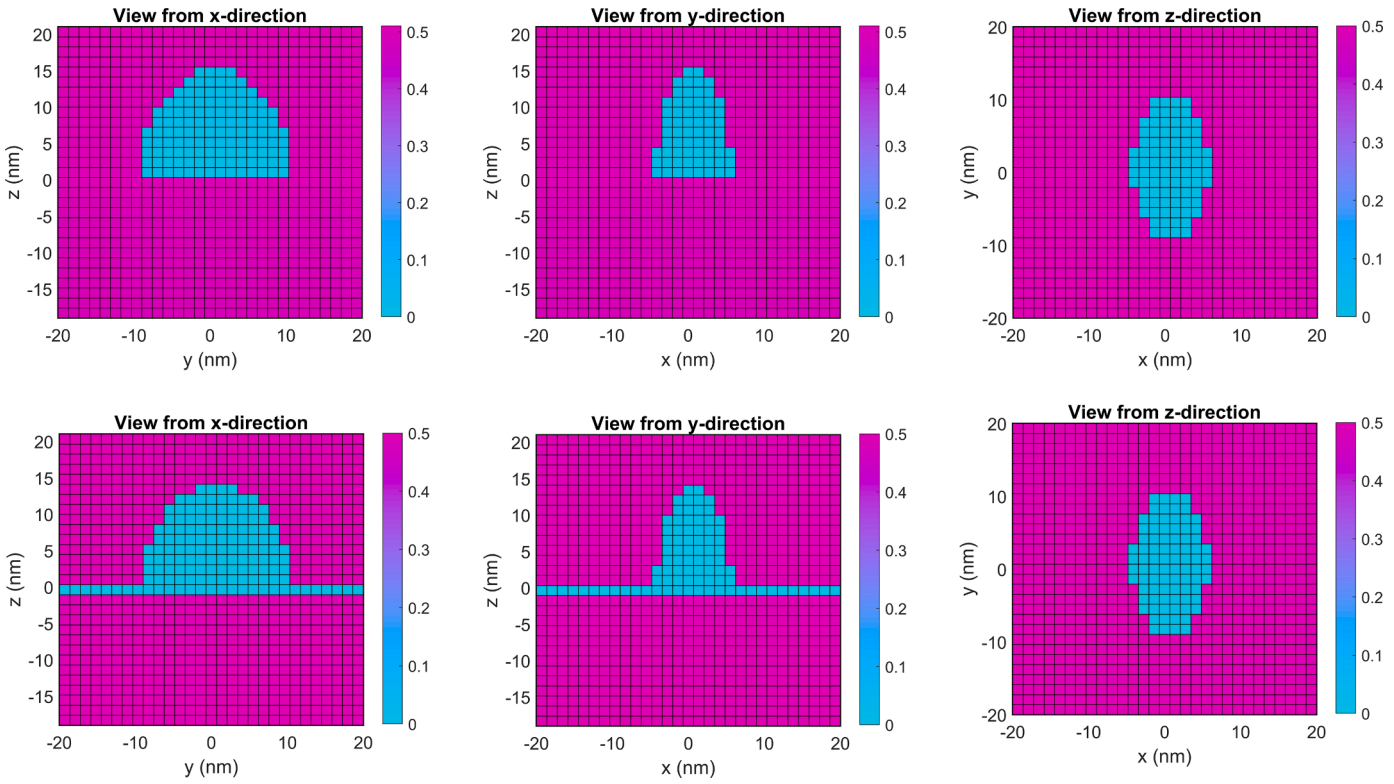

Fig. 1. Schematic cross-section of QD from *x*-axis (left), *y*-axis (middle), *z*-axis (right) for WL = 0 A (top), WL = 10 A (bottom).

of QD, optical properties were not studied at all.

In the present study, we analyze the absorption properties of semi-elliptical InAs QDs, emitting/absorbing in the THz region, surrounded by GaAs. Calculations include the WL to have more precise numerical results. In this way, the combined effect of WL thickness and electric field through axial direction has been analyzed. In particular, all results are visualized in three-dimension to do analysis covering the whole QD region, not the only center of QD to have more realistic results. In the calculations, effective mass approximation has been used and three-dimensional wavefunctions are obtained using in-home written finite element method code.

This paper is organized as follows. In section two, we describe our numerical method and explain the theory. Numerically calculated wavefunctions and corresponding energy eigenvalues are given in the results and discussion section. In subsections of results and discussion, the effect of WL thickness without an electric field on linear and nonlinear absorption properties is given. Then, three-dimensional modification of linear and nonlinear absorption are given under applied electric field through axial direction for semi-elliptical QD. We finish the paper with our conclusion in section 4.

2. Theory and method

Time-independent Hamiltonian of the three-dimensional InAs/GaAs QD heterojunction is given in Eq. (1) [19]. The electric field is set through in all directions as $\overrightarrow{F}(x, y, z) = F_x\overrightarrow{x} + F_y\overrightarrow{y} + F_z\overrightarrow{z}$. Only F_z differs from zero.

$$H = \frac{\overrightarrow{P}^2(x,y,z)}{2\ m^*} + V(x,y,z) + e\ \overrightarrow{F}(x,y,z)\cdot\overrightarrow{r}(x,y,z) \tag{1}$$

where m^* describes the effective mass of the electron and in this research, it is taken as 0.067 m_0 and 0.04 m_0 for the GaAs and InAs respectively. m_0 is the free electron mass, $\overrightarrow{p}(x,y,z)$ is the electron momentum operator, $\overrightarrow{r}(x,y,z)$ is the displacement vector, e is the electron charge, and $V(x,y,z)$ is the confinement potential. For InAs/GaAs QD system, conduction band offset and potential discontinuity $V(x,y,z)$ are taken as 0.7 and 500 meV, respectively [19]. In numerical calculations, Hamiltonian in three-dimension is written in matrix formalism as;

$$H = -\frac{h^2}{2m^*}\left(\frac{d^2}{dx^2} + \frac{d^2}{dy^2} + \frac{d^2}{dz^2}\right) + V(x,y,z) + e\ \overrightarrow{F}(x,y,z)\cdot\overrightarrow{r}(x,y,z) \tag{2}$$

where the second-order differential is defined as;

$$\frac{d^2}{dx^2} + \frac{d^2}{dy^2} + \frac{d^2}{dz^2} = \left[-2\ diag\left(ones\left(1, N_xN_yN_z\right)\right) + diag\left(ones\left(1, N_xN_yN_z - 1\right), -1\right) + diag\left(ones\left(1, N_xN_yN_z - 1\right), 1\right)\right]^2 \tag{3}$$

N_x, N_y, and N_z is the length of the matrices to define the total quantum region. To solve Eq. (2), diagonalization is used in three-dimension. After obtaining the energy levels and wave functions, linear and nonlinear absorption coefficients are calculated as follows [5]:

$$\alpha_{ij}^{(1)}(w) = w\sqrt{\frac{\mu}{\varepsilon_r}}\ \frac{\left|M_{ij}\right|^2\sigma_v h\Gamma_{ij}e^2}{\left(\Delta E_{ij} - hw\right)^2 + \left(h\Gamma_{ij}\right)^2} \tag{4}$$

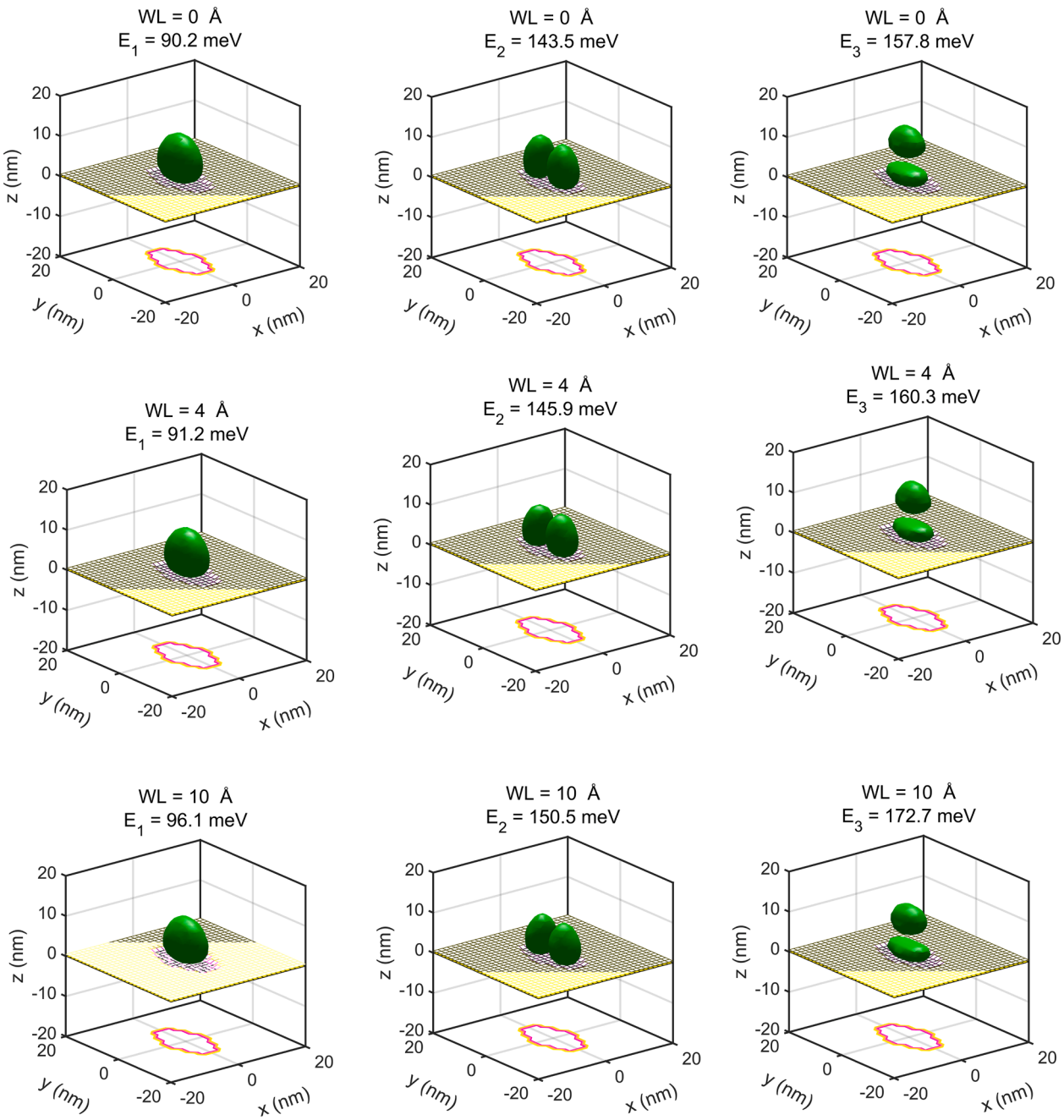

Fig. 2. Three-dimensional PDWs for different WL thickness and corresponding eigenenergies for ground, first, and second excited energy states. WL = 0 A (top), WL = 4 A (middle) and WL = 10 A (bottom).

$$\alpha_{ij}^{(3)}(w,I) = -2w\sqrt{\frac{\mu}{\varepsilon_r}}\left(\frac{I}{\varepsilon_0\, n_r\, c}\right)\frac{|M_{ij}|^4\sigma_v h\Gamma_{ij}e^4}{\left((\Delta E_{ij}-hw)^2+(h\Gamma_{ij})^2\right)^2}\left(1-\frac{|M_{ff}-M_{ii}|}{|2M_{ii}|^2}\frac{(\Delta E_{ij}-hw)^2-(h\Gamma_{ij})^2+2\Delta E_{ij}(\Delta E_{ij}-hw)}{\Delta E_{ij}{}^2+(h\Gamma_{ij})^2}\right) \quad (5)$$

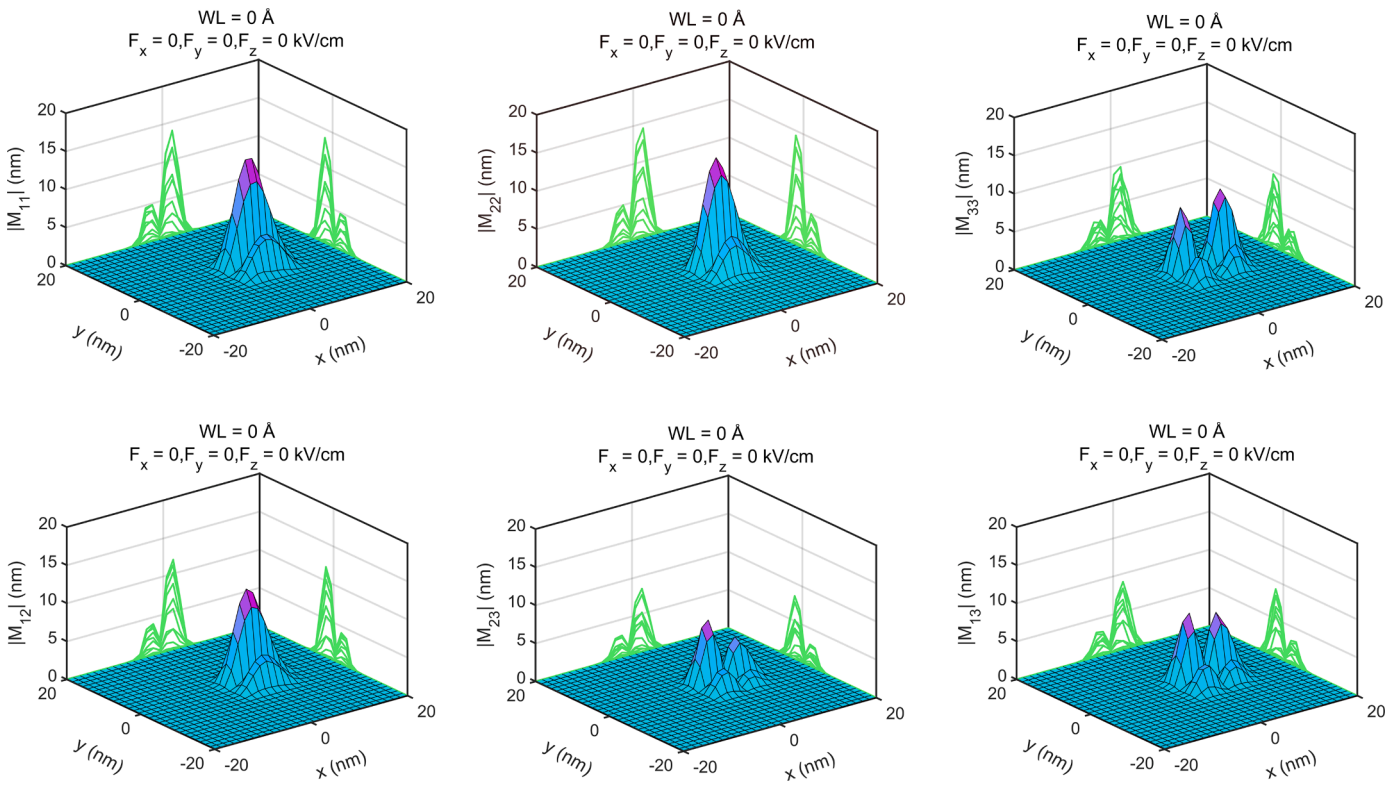

Fig. 3. Symmetric ($|M_{11}|$, $|M_{22}|$, $|M_{33}|$ upper part) and asymmetric ($|M_{12}|$, $|M_{23}|$, $|M_{13}|$ lower part) DMMEs without WL.

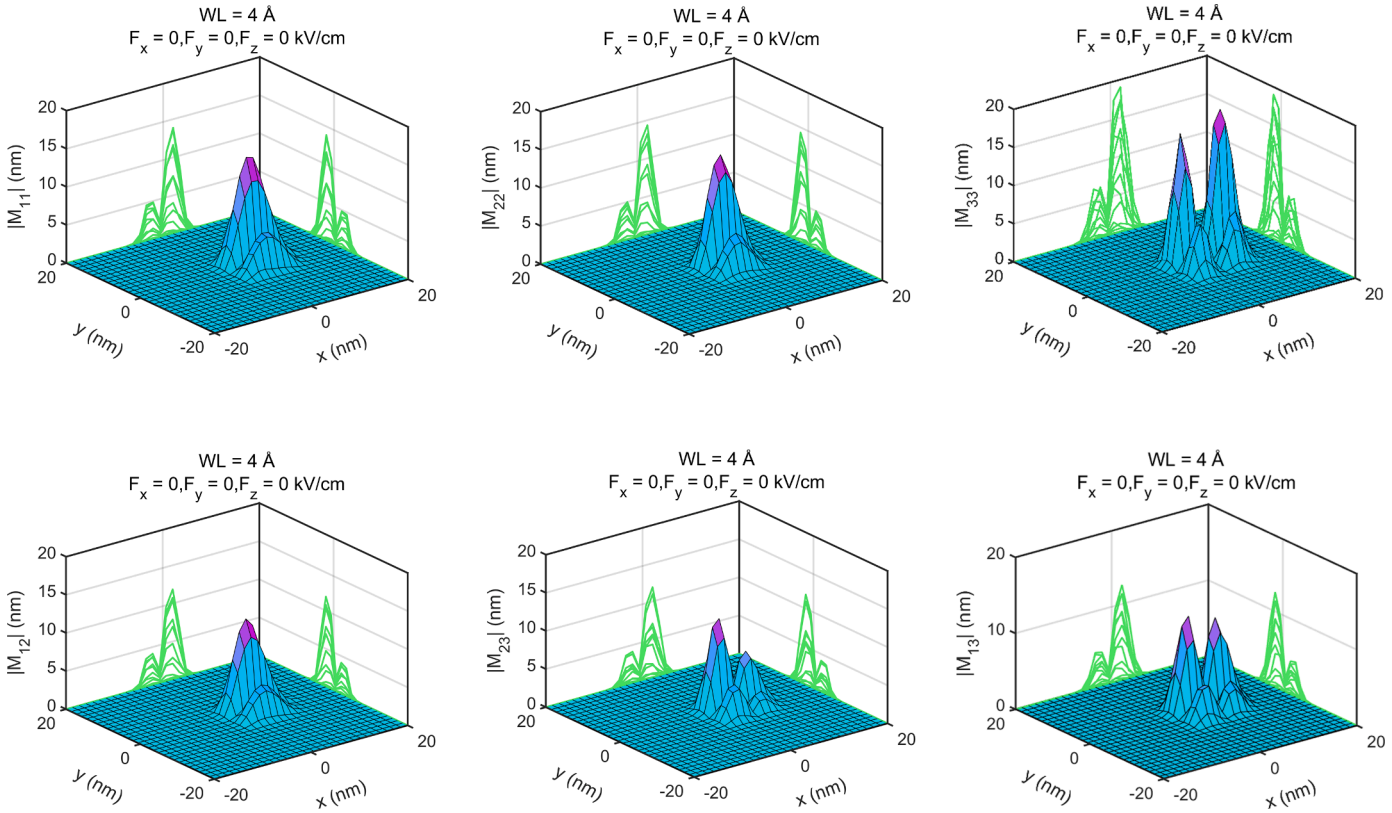

Fig. 4. Symmetric ($|M_{11}|$, $|M_{22}|$, $|M_{33}|$ upper part) and asymmetric ($|M_{12}|$, $|M_{23}|$, $|M_{13}|$ lower part) DMMEs for 4 A WL thickness.

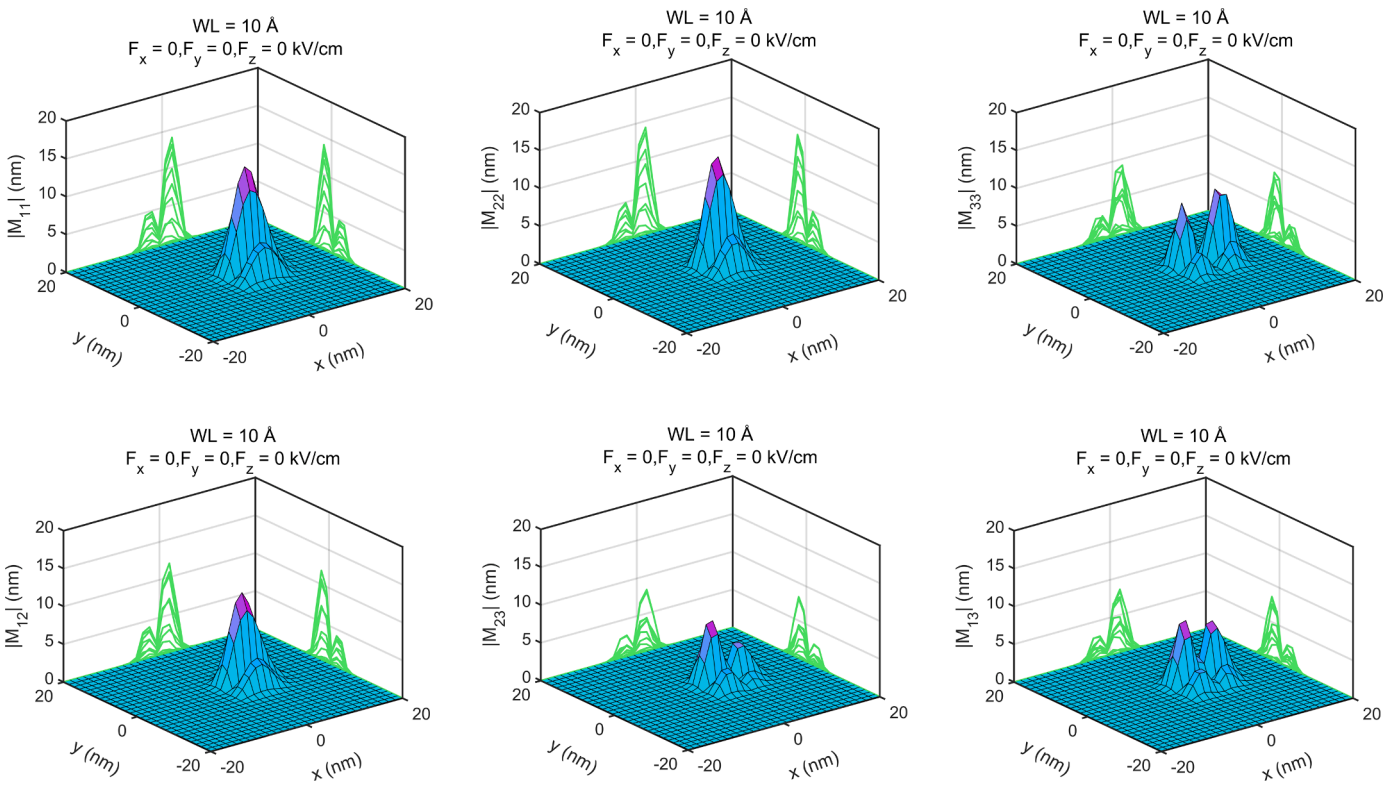

Fig. 5. Symmetric ($|M_{11}|$, $|M_{22}|$, $|M_{33}|$ upper part) and asymmetric ($|M_{12}|$, $|M_{23}|$, $|M_{13}|$ lower part) DMMEs for 10 A WL thickness.

where w is the angular frequency, Γ_{ij} is the intersubband relaxation time, μ is the magnetic permeability, ε_r is the real part of the electrical permittivity, σ_v is the carrier number, h is the reduced Planck constant and $\Delta E_{ij} = E_j - E_i$ is the energy difference between the final and initial energy levels of the electron. M_{ij} is the dipole moment matrix element (DMMEs) and it is defined as in [24];

$$M_{ij} = \langle \psi_i | \vec{r}(x, y, z) | \psi_j \rangle \tag{6}$$

Then total absorption coefficient is given as;

$$\alpha_{ij}(w, I) = \alpha_{ij}^{(1)}(w) + \alpha_{ij}^{(3)}(w, I) \tag{7}$$

3. Results and discussion

The parameters used in the study are constant and given as follows; $I = 0.1\ MW/cm^2$, $\mu = 4\pi\ x\ 10^{-7}\ H\ m^{-1}$, $\sigma_v = 2.5\ x\ 10^{17}\ cm^{-3}$, $\Gamma_{ij} = \Gamma = \frac{1}{\tau}\tau = 0.14\ ps$, and $n_r = 3.2$. Where I is the incident light intensity, μ is the permeability of the medium, τ is the transition times between states, n_r is the refractive index.

3.1. Effect of WL thickness

We run the simulations for semi-elliptical InAs QD embedded in GaAs to check our code based on the finite element method. The radii of semi-elliptical three-dimension are set as $R_x = 5$ nm, $R_y = 10$ nm and $R_z = 15$ nm to not encounter symmetry effect. WL thickness was varied from 0 to 10 A. Schematic cross-sections of QD from different aspects were shown in Fig. 1 for the WL = 0 A (top), WL = 10 A (bottom). WL layer is seen as a light blue line from *x* and *y* directions.

In Fig. 2, the three-dimensional probability density of wavefunctions (PDWs) for different WL thicknesses and corresponding eigenenergies for the ground, first, and second excited energy states (respectively E_1, E_2, and E_3) are given. Only, WL thickness for 0, 4, and 10 A are shown to avoid confusion due to many figures. The variations in the first three eigenenergies for different WL thicknesses are shown in Fig. 2 as dependent on the spatial directions to see the localization of the wavefunction in three-dimension. It is seen that obtained results are fairly in good agreement in between. The localization of wavefunctions exists only in the QD region. While PDW of the first excited state is split through the horizontal *y*-axis, PDW of the second excited state is split through the vertical *z*-axis the same as in Ref. [23]. This means that both excited states localize in different regions due to degeneracy in three-dimension. It is observed that the eigenenergies of the first three energy states are continuously increasing owing to lower confinement with increased WL thickness. In the current study, we aim to have transition energy in the THz region and we have seen that transition energies from the first and second excited states to the ground state are in the THz range. In addition, there is a slight increment between transition energies. This is due to faster scaling up of second excited state than first excited and ground states and also degeneracy extinction occurs between excited states.

DMMEs, which describe the overlap between wavefunctions, are shown without the WL in Fig. 3. Symmetric M_{11}, M_{22}, and M_{33} DMMEs are in the same scale and the magnitudes of symmetric DMMEs are comparable with reference [23]. DMME for M_{33} shows branching (double peak) even though there are no branching for M_{11} and M_{22}. This is due to the splitting of wave function through *z*-axis in three-dimension as shown in Fig. 2 for M_{33}. The magnitude of the asymmetric DMME for M_{12} is comparable with symmetric M_{11} and M_{22} however magnitude of asymmetric M_{13} is almost half of symmetric M_{33} due to lower overlap between wavefunctions. In addition to that asymmetric M_{23} and M_{13} have shown double peaks owing to the splitting of wavefunctions through the *y*-axis and *z*-axis, and also the calculation of DMME over the *z*-axis. Figs. 4 and 5 show the symmetric and asymmetric DMMEs for 4 A and 10 A WL thickness, respectively. With the effect of WL, the magnitude of the M_{33}, M_{23} and M_{13} increase at first for WL 4 A then it decreases to the same value. It is observed that this is because of the distribution of PDW, which becomes more concentrated in the center of

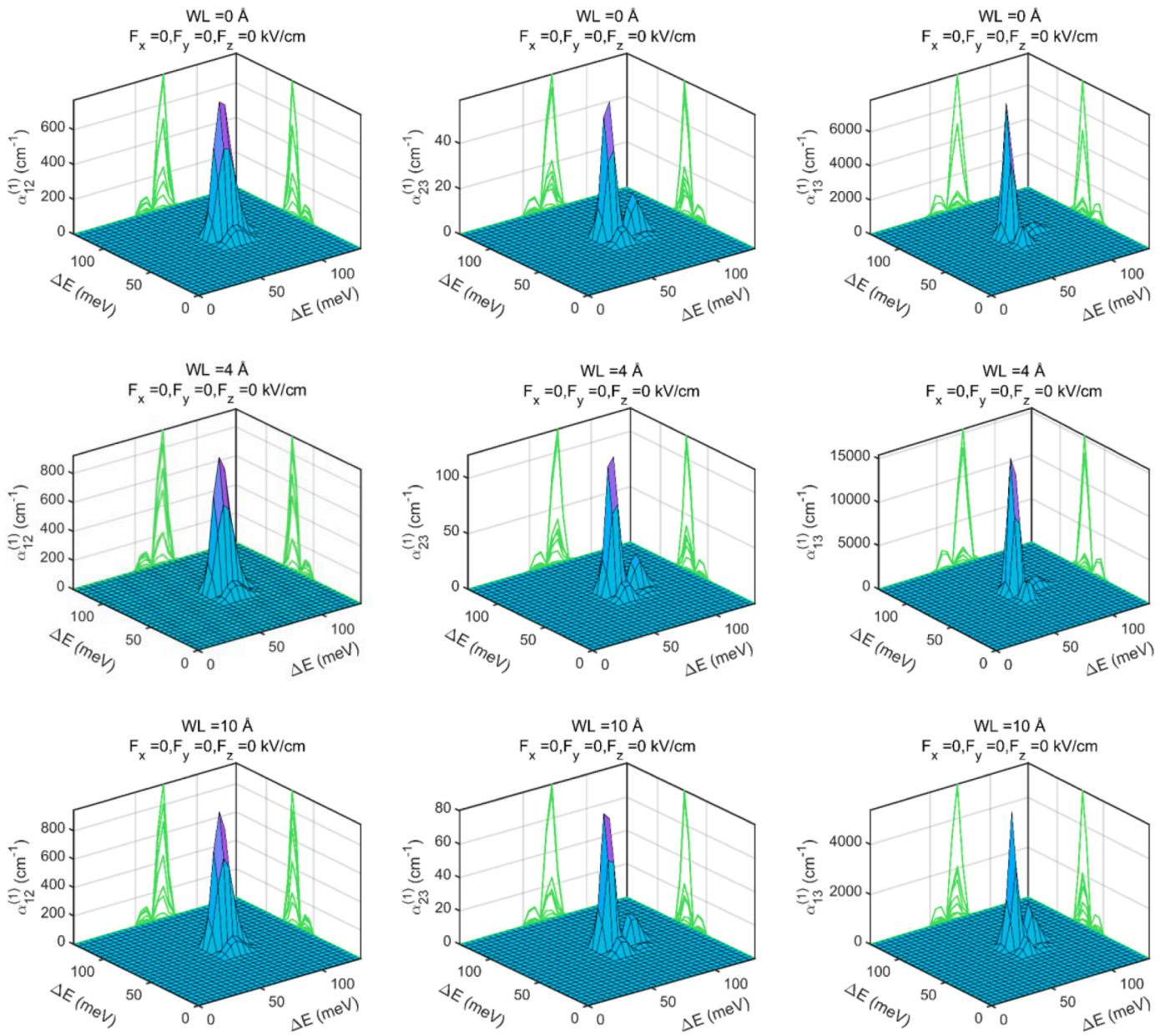

Fig. 6. LACs for different WL thicknesses WL = 0 A (top), WL=4 A (middle) and WL=4 A (bottom).

the QD for WL thickness around 4-5 A. In addition to that branching which is also observed for asymmetric M_{23} and M_{13} but it is more obvious for M_{13} at all values due to splitting of PDW.

The linear absorption coefficients (LACs) are calculated for WL thickness varied from 0 A to 10 A. In Fig. 6, linear absorption coefficients corresponding to 0, 4, and 10 A WL thickness are given for simplicity. We have seen that LAC of the (1-2) transition is not affected much by WL thickness. LAC is increasing at first then it saturates. In addition, there is dependence on WL thickness for LAC of (2-3) transition. However, WL has a huge impact on the LAC of the (1-3) transition. LAC increases more than double for WL 4 A but then decreases almost half of without WL thickness due to dependence on the DMMEs. As shown in Fig. 6, the LAC of the (1-3) transition is a lot higher than the absorption coefficient of QW structures given in the literature [25–27] due to higher confinement. LACs of the (2-3) and (1-3) transitions reach their maximum peak at 4 Å WL thickness. Another reason to have lower LAC at thick WL values, thicker WL causes lower confinement, which results in the lower overlap between PDWs. So that thicker WL causes QW-like behavior. Apart from the QD center, absorption also occurs nearby QD due to different localization directions of the wavefunction in three-dimensional space but we have not observed absorption out of the QD region due to the high confinement potential.

Nonlinear absorption coefficients (NACs) for WL thickness varied from 0 A to 10 A are also calculated. In Fig. 7, NACs only for WL thickness 0, 4, and 10 A, are given to prevent confusion. NAC of the (1-2) transition is very low and saturates at thick WL values because of the low overlap between PDWs. As shown in Fig. 7, the NAC of the (2-3) transition are zero and full noise is observed. It is seen that NAC is only exist for (1-3) transition and NAC is 100 times higher [14] even though the incident light intensity is 4 times lower comparing to the quantum wells. At the same time, NAC of the (1-3) transition has a maximum for WL around 4 A but it saturates and then drops to half of the values without WL. The nonlinear absorption peak of the (1-3) transition occurs at the center of QD due to the high confinement potential in all directions.

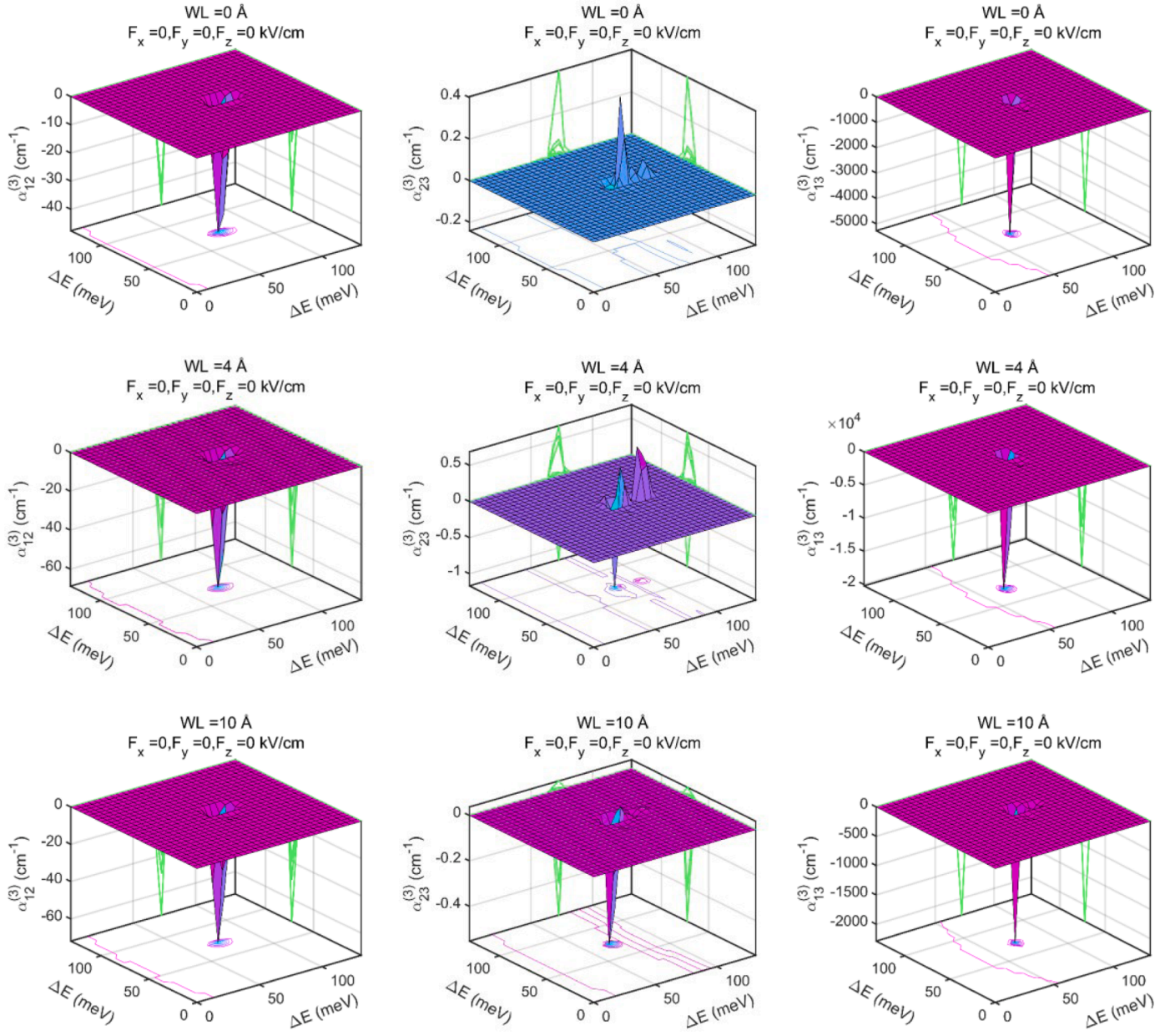

Fig. 7. NACs for different WL thicknesses WL=0 A (top), WL=4 A (middle) and WL=10 A (bottom).

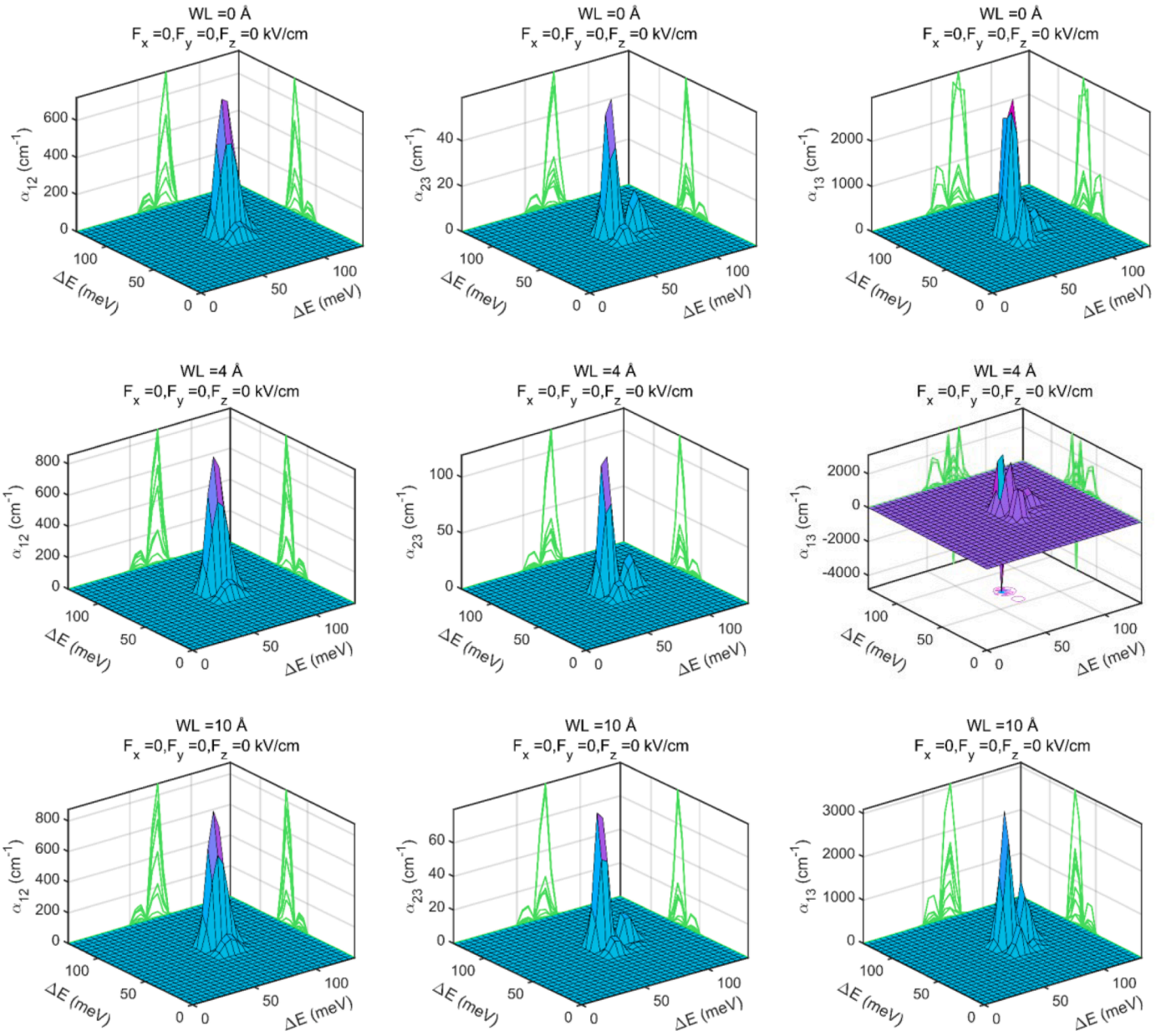

Fig. 8. Total absorption coefficients for different WL thicknesses WL=0 A (top), WL=4 A (middle) and WL=10 A (bottom).

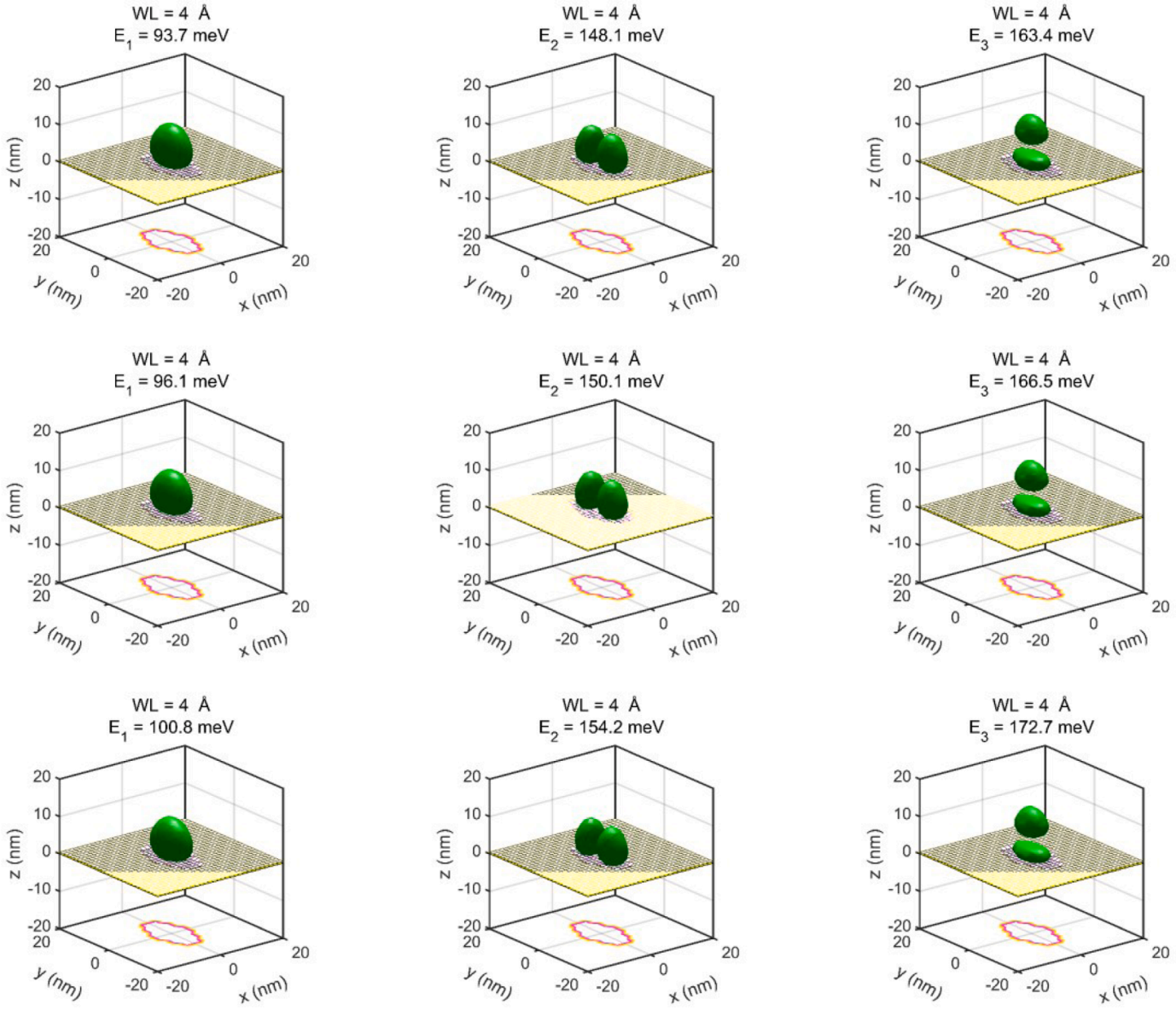

Fig. 9. Three-dimensional PDWs for different electric field intensities through axial direction for WL 4 A under electric field for 5 kV/cm (top), 10 kV /cm (middle) and 20 kV/cm (bottom).

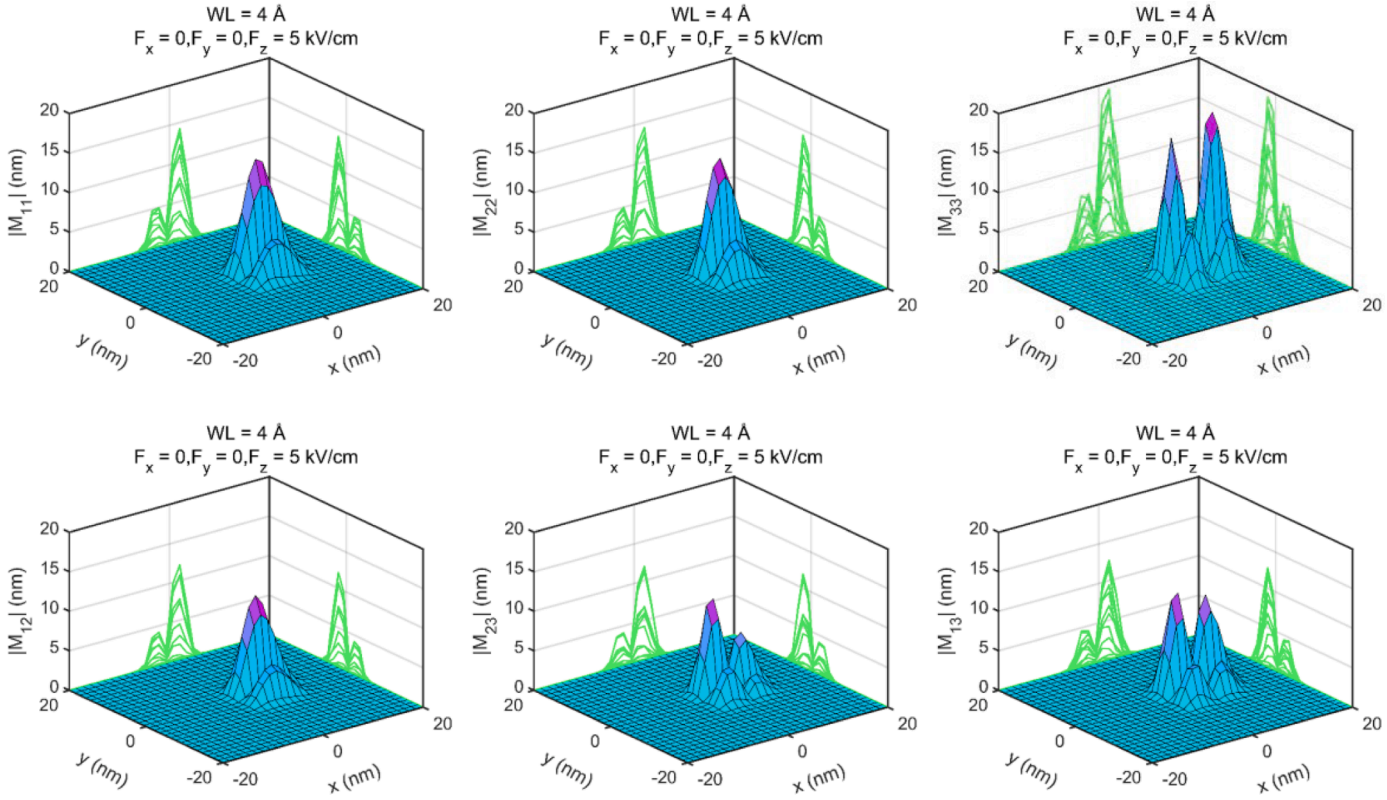

Fig. 10. DMMEs for electric field intensity at 5 kV/cm applied through axial direction for WL=4 A.

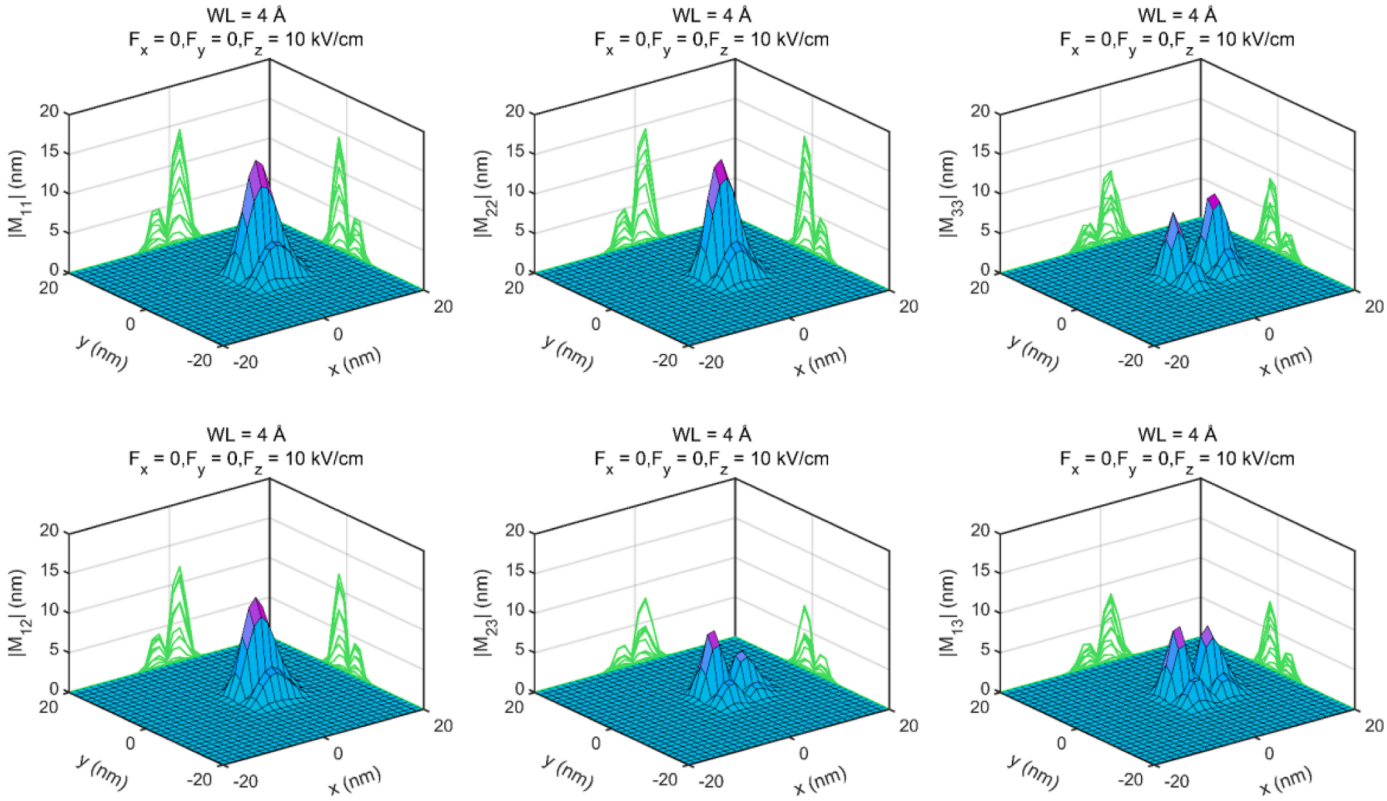

Fig. 11. DMMEs for electric field intensity at 10 kV/cm applied through axial direction for WL = 4 A.

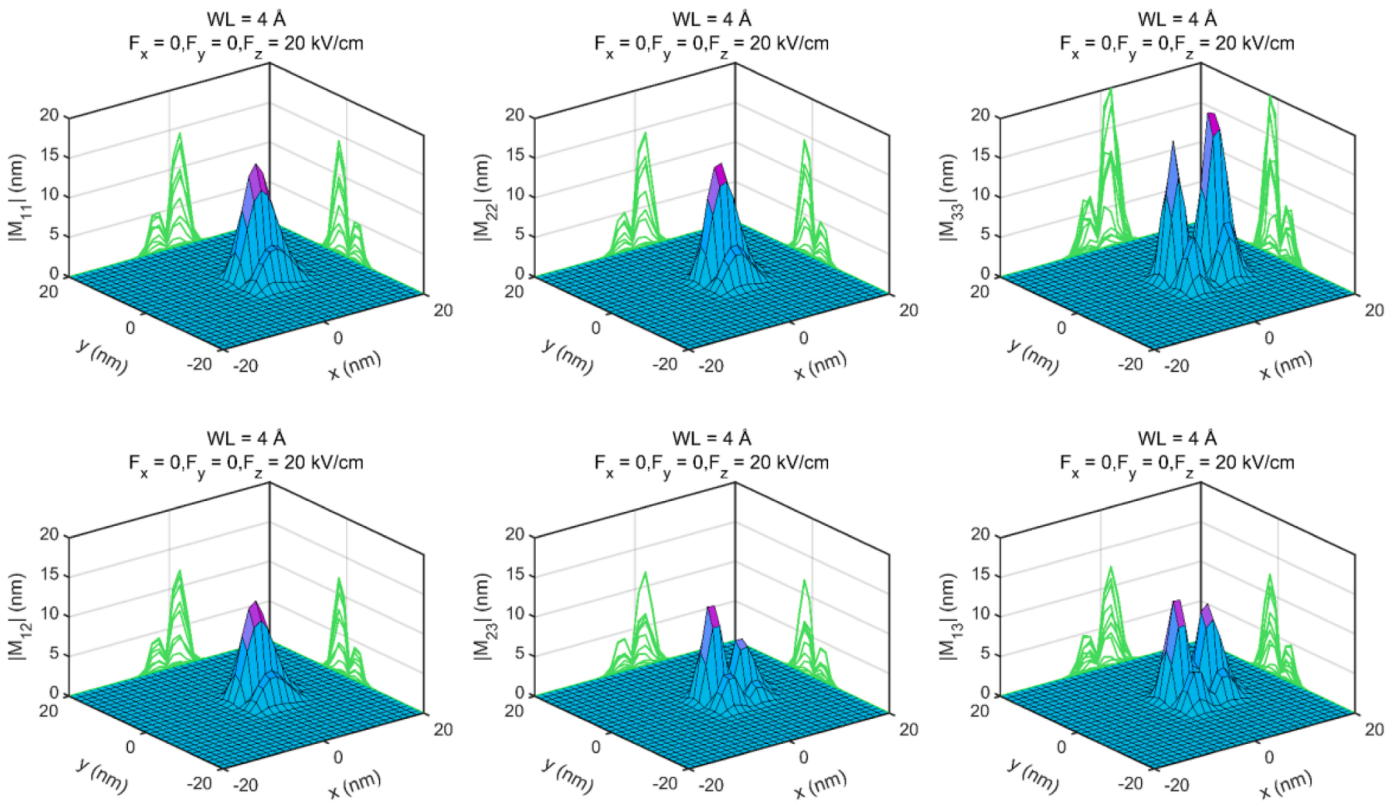

Fig. 12. DMMEs for electric field intensity 20 kV/cm applied through axial direction for WL = 4 A.

Total absorption coefficients (TACs) for several WL thicknesses varying from 0 A to 10 A are given in Fig. 8. Due to weak NAC for (1-2) and (2-3) transitions, LAC is the dominant mechanism that results in slightly different TACs than LACs for all WL thicknesses. TACs of (1-3) transition are positive for WL 0 and 10 A owing to dominant LAC for thin and thick WLs, but TAC is branching for WL thickness of 4 A because of strong NAC. This also results in branching as shown in Fig. 8 (middle).

3.2. *Effect of axial electric field*

We have studied the effect of the electric field applied through axial direction on optical properties of InAs/GaAs semi-elliptical QD. We have set WL thickness to 4 A and changed the electric field intensity from 5 to 20 kV/cm while other parameters are constant. PDW and corresponding energy eigenvalues to the first three energy states are given in Fig. 9 in three-dimensional plots. Energy eigenvalues are shifting up with the effect of the electric field. However, the electric field has no effect on the splitting direction or shapes of PDWs. It is seen that PDW of carriers is restricted to a smaller area than QD size for all energy states. This is crucial for electronic and optoelectronic applications due to prevent carrier leakage. While (1-2) transition energy is slightly inversely proportional with electric field intensity due to the faster shift of the ground state energy to higher energies, there is a small increment in transition energies for the (2-3) and (1-3) under applied electric field.

In Figs. 10–12, DMMEs are given for different electric field intensities. M_{11} and M_{22} are constant and independent from the applied electric field. But M_{33} drops to half at 10 kV/cm then higher electric field intensity (20 kV/cm) results in high DMME. Furthermore, electric field enhances branching in M_{33}, it is less pronounced in the case of zero electric fields for varied WL thickness. M_{12} is also constant and behaves the same as M_{11} and M_{22}. M_{23} have a dip around 10 kV /cm because of the PDW of the second excited state. M_{13} has the same values for 5 and 20 kV/cm as in the absence of an electric field, only 2 times lower for 10 kV/cm.

LACs for electric field intensities varying from 0to 20 kV/cm are calculated. In Fig. 13, LACs are plotted for different electric field intensities. As expected LAC of the (1-2) transition is almost very low due to low DMME. We have seen that LAC is very low for (2-3) transition as well for all electric field intensities and there is a minimum peak for 10 kV/cm, which is originating from DMME. Even though LAC of (1-2) and (2-3) transitions are low, LAC of (1-3) is very strong and this is due to DMME, but LAC has a minimum (maximum) peak around 10 kV/cm (20 kV/cm).

NACs for electric field intensities varying from 5, 10 and 20 kV/cm are shown in Fig. 14. As seen from this figure, these absorption coefficients are constant for (1-2) transition and independent from electric field intensity. NACs are zero for (2-3) transition and noise is observed in all, we think that it is because of the distribution of PDW of first and second excited states through different directions. As happened in LAC, NACs of (1-3) transition are very strong even though it is decreasing with electric field intensity at first. At 20 kV/cm electric field intensity, it has maximum values owing to the enhanced overlap of wavefunctions. At the same time, very small nonlinear absorption has been observed at lower transition energy, and nonlinear absorption is notable close to the QD center.

TACs for electric field intensities varying from 5, 10 and 20 kV/cm are shown in Fig. 15. As a result of independent LAC and NAC from the electric field for (1-2) transition, TAC is also independent. Low LAC and NAC result in low TAC for (2-3) transition. Due to the low perturbation effect of nonlinear properties, for (1-3) transition, LAC is dominant for 10 kV/cm and the maximum of TAC is half of the LAC. The presence of great NAC causes branching in the TAC at 5 and 20 kV/cm intensities. Additionally, positive and negative TACs are observed due to the same reason.

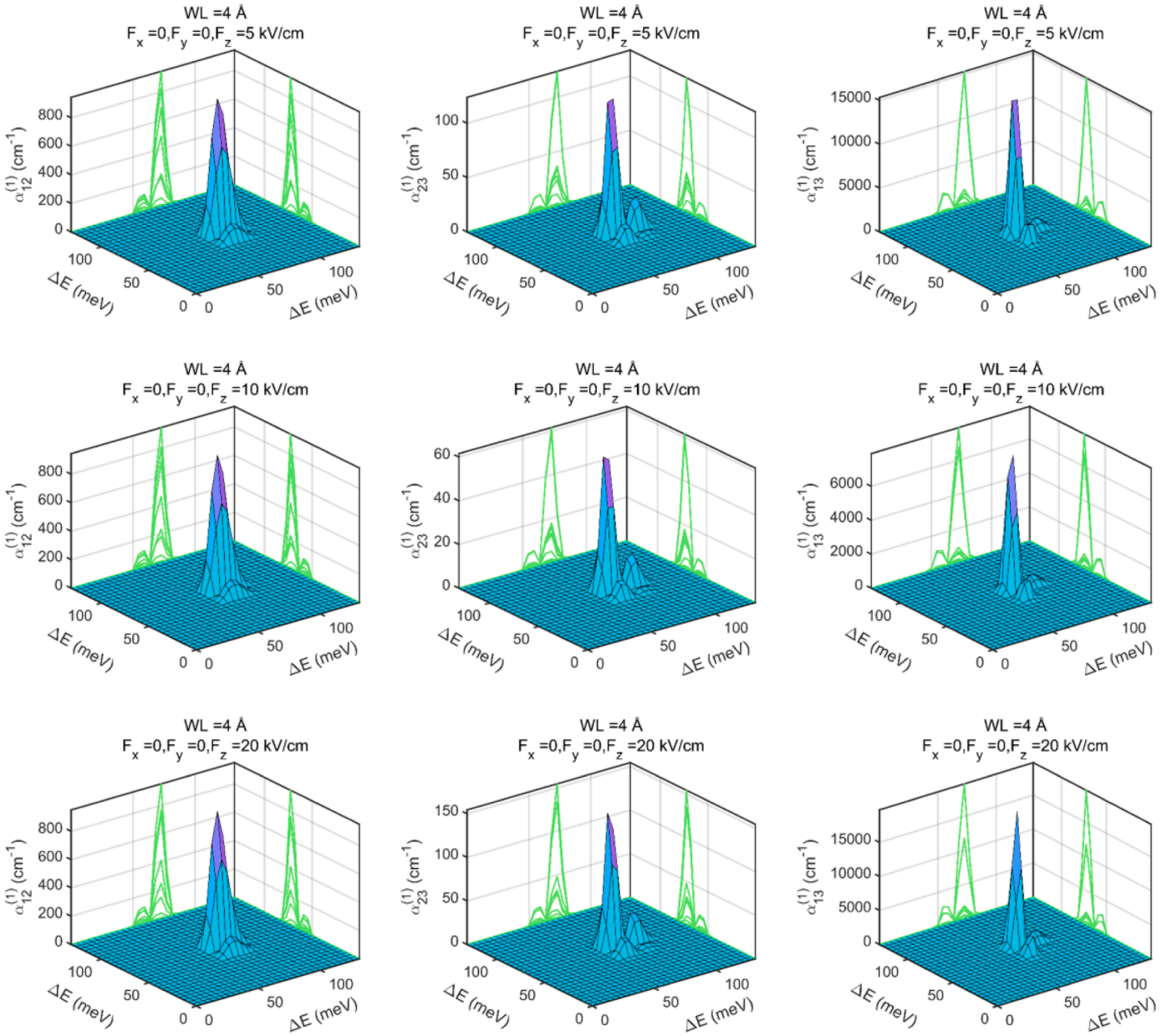

Fig. 13. LACs for electric field intensities F = 5 kV/cm (top), F = 10 kV/cm (middle), F = 20 kV/cm (bottom) for WL = 4 A.

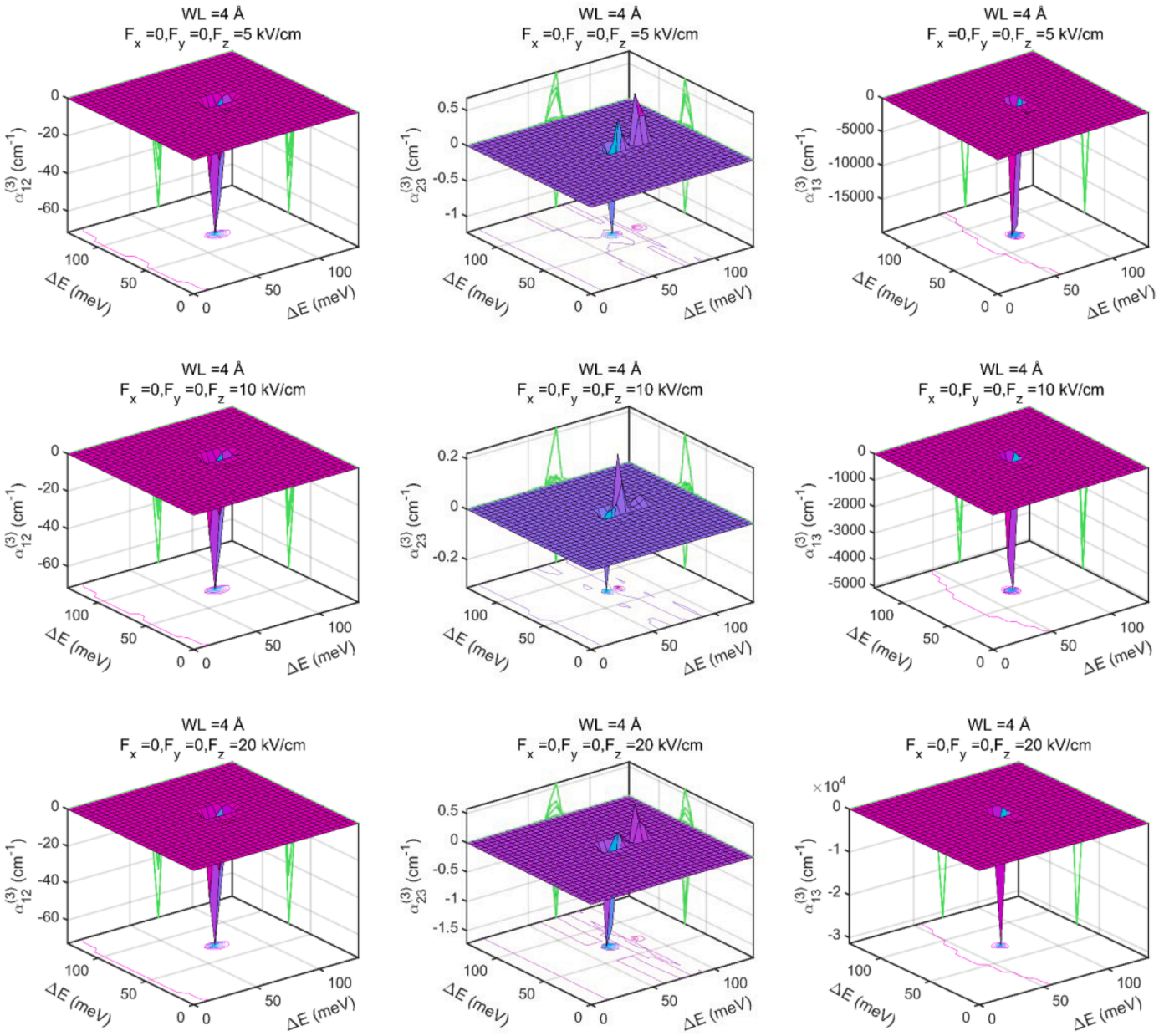

Fig. 14. NACs for electric field intensities F = 5 kV/cm (top), F = 10 kV/cm (middle), F = 20 kV/cm (bottom) for WL = 4 A.

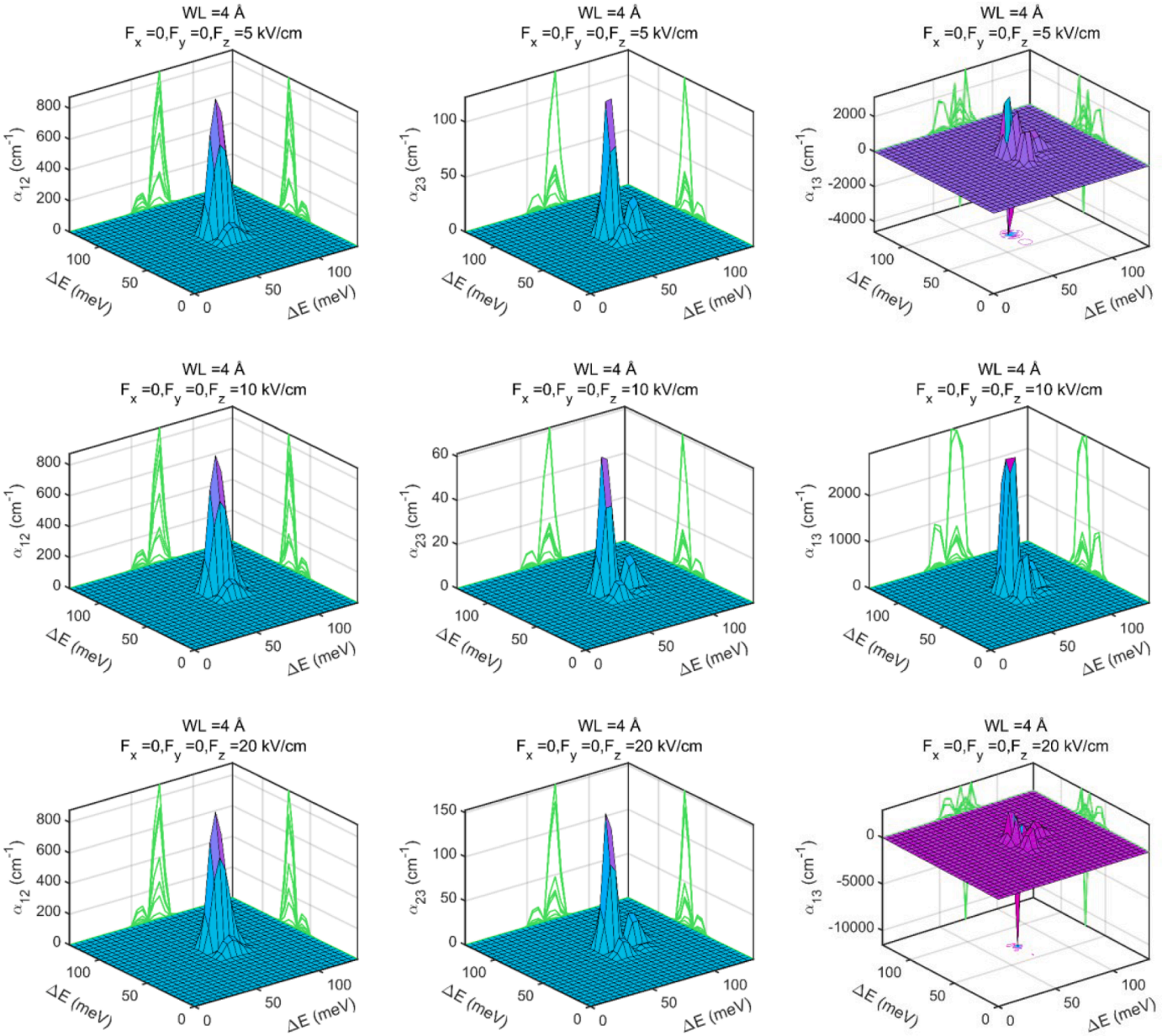

Fig. 15. TACs for electric field intensities F = 5 kV/cm (top), F = 10 kV/cm (middle), F = 20 kV/cm (bottom) for WL = 4 A.

Conclusion

In the present article, we have studied the linear, nonlinear and total absorption properties of semi-elliptical InAs QD surrounded by high bandgap GaAs and aimed to give brief guidance to design semi-elliptical InAs QD semiconductor devices, operating in the THz region, based on optical transitions. We have shown linear, nonlinear, and total absorption coefficients in three-dimension. We have studied the effect of WL thickness varying from 0 and 10 A in the case of zero electric field intensity. We observe that energy eigenvalues shift to upper energy values with WL thickness due to lower confinement. While there is no branching (double peak) for symmetric M_{11} and M_{22}, branching is observed for M_{33} because of the splitting of PDW in three-dimensional space. This is not observable in the one-dimensional analysis of the QD structures. It is found that while M_{12} is not affected by a change in WL thickness, M_{23} and M_{13} becomes maximum for 4 A WL. The variation of LAC, NAC and TAC for (1-2) and (2-3) transitions are small depending on the energy differences and DMMEs. However, a strong absorption occurs for (1-3) transition due to strong DMMEs. We can say that to design a semi-elliptical QD-based semiconductor device, only optical transition E_{13} can be used. For light-emitting diodes or laser designs, the wavelength range that is reached by E_{13} transition can be obtained. To design semiconductor saturable absorber mirror (SESAM), E_{13} transition can be used to absorb the light but E_{12} and E_{23} transition can be used to refresh the reflectance of the SESAM. After determination of the effect of the WL thickness, we have set WL to 4 A and applied an electric field through the axial direction (z-direction). There is small change in transition energy of (1-2) and (2-3) with the applied electric field but transition energy is slightly increasing for (1-3). While LAC of (1-2) and (2-3) transitions are low, LAC of (1-3) is very strong due to DMMEs. For 20 kV/cm electric field intensity, LAC reaches the maximum for the (2-3) and (1-3) transition. This is due to the overlapping of the wavefunctions due to the different distribution of PDWs. We have seen that TAC of (1-3) transition shows branching and even positive and negative values due to negative NAC. As a conclusion, we can say that optical properties of InAs QD embeded in GaAs can be tuned by using WL thickness and electric field to design QD based optical semiconductor device.

Credit author statement

We all confirm that last version of the paper is seen by all of us. The text, figures and all part of the paper is checked multiple time.

First and corresponding author: Dr. Behçet Özgür Alaydin, contributed all part of the paper.

Coauthor: Asst. Prof. Dr. Didem Altun had contribution at simulation, plotting and writing.

Coauthor: Prof. Dr. Emine Öztürk had contribution in writing, editing and data treatment.

Declaration of Competing Interest

The authors declare that they have no known competing financial interests or personal relationships that could have appeared to influence the work reported in this paper.

Acknowledgments

This study was partly funded by the Scientific and Technological Research Council of Turkey (TUBITAK) ARDEB 1005 Grant No 121F013 and supported by Sivas Cumhuriyet University Scientific Research Project (F-2021-647).

Reference

[1] M. Gaulke, J. Heidrich, B. Özgür Alaydin, M. Golling, A. Barh, U. Keller, High average output power from a backside-cooled 2-μm InGaSb VECSEL with full gain characterization, Opt. Express 29 (2021) 40360–40373.
[2] H. Hu, S. Zhou, X. Liu, Y. Gao, C. Gui, S. Liu, Effects of GaN/AlGaN/Sputtered AlN nucleation layers on the performance of GaN-based ultraviolet light-emitting diodes, Sci. Rep. 7 (2017) 44627.
[3] M.M. Ackerman, X. Tang, P. Guyot-Sionnest, Fast and sensitive colloidal quantum dot mid-wave infrared photodetectors, ACS Nano 12 (2018) 7264–7271.
[4] J. Heidrich, M. Gaulke, B.O. Alaydin, M. Golling, A. Barh, U. Keller, Full optical SESAM characterization methods in the 1.9 to 3-μm wavelength regime, Opt. Express 29 (2021) 6647–6656.
[5] B.O. Alaydin, Effect of high bandgap AlAs quantum barrier on electronic and optical properties of In0.70Ga0.30As/Al0.60In0.40As superlattice under applied electric field for laser and detector applications, Int. J. Mod. Phys. B 35 (2020), 2150027.
[6] M.G. Barseghyan, C.A. Duque, E.C. Niculescu, A. Radu, Intense laser field effects on the linear and nonlinear optical properties in a semiconductor quantum wire with triangle cross section, Superlattices Microstruct. 66 (2014) 10–22.
[7] S. Nasa, S.P. Purohit, Linear and third order nonlinear optical properties of GaAs quantum dot in terahertz region, Phys. E Low Dimens. Syst. Nanostruct. 118 (2020), 113913.
[8] M. Paul, P. Bhattacharya, B. Das, S. Rani, Effects of external electric and magnetic fields on the linear and nonlinear optical properties of InAs cylindrical quantum dot with modified Pöschl-Teller and Morse confinement potentials, J. Electr. Electron. Eng. Res. 126 (2021), 114440.
[9] B.O. Alaydin, E. Ozturk, S. Elagoz, Interband transitions dependent on indium concentration in Ga1−xInxAs/GaAs asymmetric triple quantum wells 32 (2018), 1850052.
[10] I. Altuntas, Effects of applied external fields on the nonlinear optical rectification, second, and third harmonic generation in a quantum well with exponentially confinement potential, Eur. Phys. J. B 94 (2021) 177.
[11] O. Ozturk, B.O. Alaydin, D. Altun, E. Ozturk, Intense laser field effect on the nonlinear optical properties of triple quantum wells consisting of parabolic and inverse-parabolic quantum wells, Laser Phys. 32 (2022), 035404.
[12] İ. Karabulut, Ü. Atav, H. Şafak, M. Tomak, Linear and nonlinear intersubband optical absorptions in an asymmetric rectangular quantum well, Eur. Phys. J. B 55 (2007) 283–288.
[13] E. Ozturk, H. Sari, I. Sokmen, The dependence of the intersubband transitions in square and graded QWs on intense laser fields, Solid State Commun. 132 (2004) 497–502.
[14] B.Ö. Alaydin, Optical properties of GaAs/AlxGa1-xAs superlattice under E-field for quantum cascade laser application, Gazi Univ. J. Sci. 34 (2021) 1179–1191.
[15] A. Khaledi-Nasab, M. Sabaiean, M. Sahrai, V. Fallahi, Optical rectification and second harmonic generation on quasi-realistic InAs/GaAs quantum dots: with attention to wetting layer effect, ISRN Condens. Matter Phys. (2013), 530259, 2013.
[16] M. Cristea, A. Radu, E.C. Niculescu, Electric field effect on the third-order nonlinear optical susceptibility in inverted core–shell nanodots with dielectric confinement, J. Lumin. 143 (2013) 592–599.
[17] W. Xie, The nonlinear optical rectification coefficient of quantum dots and rings with a repulsive scattering center, J. Lumin. 143 (2013) 27–30.
[18] M. El Haouari, A. Talbi, E. Feddi, H. El Ghazi, A. Oukerroum, F. Dujardin, Linear and nonlinear optical properties of a single dopant in strained AlAs/GaAs spherical core/shell quantum dots, Opt. Commun. 383 (2017) 231–237.
[19] M. Choubani, H. Maaref, F. Saidi, Nonlinear optical properties of lens-shaped core/shell quantum dots coupled with a wetting layer: effects of transverse electric field, pressure, and temperature, J. Phys. Chem. Solids 138 (2020), 109226.
[20] M. Chnafi, A. El Moussaouy, O. Mommadi, L. Belamkadem, Energy and stability of negatively charged trion in cylindrical quantum dot under temperature effect, Phys. B Condens. Matter 594 (2020), 412333.
[21] A.M. Maniero, C.R. de Carvalho, F.V. Prudente, G. Jalbert, Effect of a laser field in the confinement potential of two electrons in a double quantum dot, J. Phys. B At. Mol. Opt. Phys. 52 (2019), 095103.
[22] A. Boda, Magnetic moment and susceptibility of an impurity in a parabolic quantum dot, J. Magn. Magn. Mater. 483 (2019) 83–88.
[23] J.A. Osorio, D. Caicedo-Paredes, J.A. Vinasco, A.L. Morales, A. Radu, R.L. Restrepo, J.C. Martínez-Orozco, A. Tiutiunnyk, D. Laroze, N.N. Hieu, H.V. Phuc, M.E. Mora-Ramos, C.A. Duque, Pyramidal core-shell quantum dot under applied electric and magnetic fields, Sci. Rep. 10 (2020) 8961.
[24] H. Dakhlaoui, I. Altuntas, M.E. Mora-Ramos, F. Ungan, Numerical simulation of linear and nonlinear optical properties in heterostructure based on triple Gaussian quantum wells: effects of applied external fields and structural parameters, Eur. Phys. J. Plus 136 (2021) 894.
[25] S. Baskoutas, C. Garoufalis, A.F. Terzis, Linear and nonlinear optical absorption coefficients in inverse parabolic quantum wells under static external electric field, Eur. Phys. J. B 84 (2011) 241–247.
[26] A. Doyeol, C. Shun-lien, Calculation of linear and nonlinear intersubband optical absorptions in a quantum well model with an applied electric field, IEEE J. Quantum Electron. 23 (1987) 2196–2204.
[27] E. Ozturk, I. Sokmen, Intersubband transitions in an asymmetric double quantum well, Superlattices Microstruct. 41 (2007) 36–43.